NASA

Technical Memorandum 85044

OBSERVATIONS OF THE 10 MICROMETER NATURAL LASER EMISSION FROM THE MESOSPHERES OF MARS AND VENUS

D. Deming
F. Espenak
D. Jennings
T. Kostiuk
M. Mumma

JUNE 1983

National Aeronautics and
Space Administration

Goddard Space Flight Center
Greenbelt, Maryland 20771

OBSERVATIONS OF THE 10-MICROMETER NATURAL LASER EMISSION FROM THE MESOSPHERES OF MARS AND VENUS

D. Deming*, F. Espenak, D. Jennings*, T. Kostiuk*, and M. Mumma*
Infrared and Radio Astronomy Branch
NASA/Goddard Space Flight Center
Greenbelt, MD 20771

and

D. Zipoy
Astronomy Program
University of Maryland
College Park, MD 20742

Proofs and Correspondence to:

Drake Deming
Code 693, Goddard Space Flight Center
Greenbelt, MD 20771

Suggested running head: observations of natural laser emission

*Visiting Astronomer at Kitt Peak National Observatory, which is operated by the Association of Universities for Research in Astronomy under contract with the National Science Foundation.

ABSTRACT

Non-thermal emission occurs in the cores of the 9.4 and 10.4μm CO_2 bands on Mars, and has been recently identified as a natural atmospheric laser. This paper presents observations of the total flux and center-to-limb dependence of this emission for Mars and Venus. The emission is believed to be excited by absorption of solar flux in the near-IR CO_2 bands, followed by collisional transfer to the $00^0 1$ state of CO_2. A comparison is made between the observations and a detailed theoretical model based on this mechanism. It is found that the theoretical model successfully reproduces the observed center-to-limb dependence of this emission, to within the limits imposed by the spatial resolution of the observations. A comparison is also made between the observed fluxes and the predictions of the theoretical models. The observed flux from Mars agrees closely with the prediction of the model; the flux observed from Venus is 74% of the flux predicted by the model.

We utilize this emission to obtain the kinetic temperatures of the Martian and Venusian mesospheres. For Mars near 70 km altitude, a rotational temperature analysis using five lines gives T = 135 ± 20K. The frequency width of the emission is also analyzed to derive a temperature of 126± 6K. In the case of the Venusian mesosphere near 109 km, the frequency width of the emission gives T = 204±10K.

I. INTRODUCTION

Strong non-thermal emission in the 9.4 and 10.4μm bands of CO_2 was first reported for the atmospheres of Mars and Venus by Betz et al. (1976), Johnson et al. (1976) and Betz (1976) using infrared heterodyne spectroscopy. The emission occurs in the cores of the CO_2 absorption lines and is only detectable at spectral resolving powers of $\gtrsim 10^6$. The emission is believed to be formed by absorption of near-infrared solar flux, followed by collisional transfer of the absorbed quanta to the 00^01 level of CO_2, and radiative decay at 10μm (Johnson et al. 1976; Betz 1976). The emission disappears in the absence of sunlight (Deming et al. 1982). Recently, Mumma et al. (1981) have demonstrated that in the case of Mars this emission arises from a population inversion, making it a natural laser. The emission intensity was reported by Betz (1976) and Betz et al. (1976) to be approximately proportional to tne incident solar flux, but little attempt was made to quantify this dependence. The understanding of this emission and its implications is still not complete. Until now, no complete comparison has been made between observations and the predictions of a suitably detailed theoretical model.

This paper presents extensive observations of this emission from the mesospheres of Mars and Venus. We obtain the total flux emitted in the 9.4 and 10.4μm bands and the center-to-limb dependence of the emergent intensity. These quantities are compared to the predictions of a detailed theoretical model (Deming and Mumma, 1983). We obtain the kinetic temperature in the Martian mesosphere near 70 km from the frequency width of this emission and from a rotational temperature analysis.

II. OBSERVATIONS

Observations of the emission in lines of the $[(10^00)-(02^00)]$, I and II bands were made using the Goddard Space Flight Center infrared heterodyne spectrometer and the Kitt Peak National Observatory McMath main solar telescope during several observing runs from December 1979 through April 1980. The spectrometer is described in detail by Kostiuk et al. (1980) and Mumma et al. (1982). Observations were made of Mars near opposition and of Venus near

phase 0.5; the Venus observations (Fig. 1) are of higher quality than the Mars observations because the emission was much brighter and the planetary disk was much larger than the 1.7 arc-sec FWHM instrumental field of view, allowing better spatial resolution. Most of the observations were made in the 10.3337 μm R(8) line, but other lines were also observed. The observations were made at two spectral resolutions: 25 MHZ (0.0008 cm^{-1}) and 5 MHZ (0.000017 cm^{-1}), using two separate RF filter banks. For comparison, the Doppler half-width at half-maximum for CO_2 lines at 150K is 19 MHZ. The 25 MHZ and 5 MHZ data were registered simultaneously; the 5 MHZ filter bank was tunable and was centered on the emission core. For all of these observations, terrestrial CO_2 absorption was present at the frequency of the CO_2 laser local oscillator, and was defined and removed by observing the Moon, which is a thermal continuum source at this frequency. The observations were calibrated in terms of absolute flux, above the atmosphere, by adopting an appropriate temperature for the observed location on the lunar surface (Montgomery et al. 1966). For the planetary observations, the position of the beam was established by visual inspection of the image on a television monitor. Under conditions of good seeing we found that the beam center position can be set in this manner to a precision of ~1 arc-sec. This visually estimated position was later corrected for the (small) differential refraction between the visual and 10μm regions. This correction was made based on the indices of refraction for air at continuum frequencies. The aspect geometries of the planetary disks were used to compute the angular distance of each observed point from the sub-Earth and sub-solar points.

III. ANALYSIS

Each observation of the emission line yields three quantities: the frequency width of the line, the line center frequency, and the specific intensity of the emission core (ergs cm^{-2} sec^{-1} sr^{-1}). We obtain these quantities by fitting a gaussian to the observed emission core, after stripping off the underlying absorption profile. This removal of the absorption profile was facilitated in the case of Mars by obtaining a model atmosphere fit to the absorption line. The absorption line profile was modelled as the sum of transmitted thermal radiation from the surface and the

self-emission of the overlying atmosphere. The surface temperature was obtained from the observed line profile by fitting to the flux in the far wings, where the atmosphere is optically thin. A temperature vs. altitude profile, appropriate to the local time and season, was adopted based on the discussion of Seiff (1978). The CO_2 line parameters used in calculating the line profile are well known, and were taken from McClatchey et al. (1973) and Freed et al. (1980). The atmospheric surface pressure was treated as a free parameter and was varied in order to obtain an optimal fit to the observed line. Surface pressures derived in this way were consistent with the variations given in Viking ground-truth results (Hess et al. 1980). Examples of the modelling and removal of the underlying absorption profile are given on Fig. 2. Further discussion of the absorption line fitting process is not given here, because the results for the emission core are not sensitive to the details of this procedure. In the case of Venus the emission completely dominates the underlying absorption profile, which is so shallow that it can be ignored.

a) Kinetic temperatures

We derive kinetic temperatures for the emitting region by attributing the frequency width of the observed line to molecular thermal motion. In actual practice the derived kinetic temperatures are only upper limits, since other effects act to broaden the line. These effects include planetary rotation and atmospheric turbulence within the heterodyne field of view, possible local oscillator drift, and the finite resolution of the RF filters. During each observation there is also a change in the line of sight component of the earth's rotational velocity. The frequency widths derived for the emission core were corrected for this latter effect when it was appreciable. It is assumed in this procedure that gain-narrowing of the line profile due to stimulated emission is a negligible effect. The theoretical model of the emission (Deming and Mumma 1983) supports this assumption.

Kinetic temperatures were derived in this way only for lines in the 10.4μm band. For the better Mars data the error associated with a single such temperature determination is ±8K; the Venus data has smaller errors. However,

we find variations of ~±30K from our Mars measurements, so we may be observing real temperature fluctuations (e.g. Zurek, 1976). Using this technique, we obtain average temperatures for the mesospheres of Mars and Venus of 126 ± 6K and 204 ± 10K at 70 and 109 km respectively. The individual measurements are given in Tables I and II.

b) Rotational temperatures

Since we expect the rotational levels of CO_2 to be in thermal equilibrium at the pressures of relevance here, we can use observations of the emission from a range of rotational levels to determine the rotational temperature of the mesospheres. We have done this in the case of Mars by observing the emission from 6 lines with J-values ranging from 4 to 26. In the case of the R(26) line the emission core is very weak and the value we obtain for the integrated emission is sensitive to the manner in which the underlying absorption profile is modelled. This line was therefore omitted from the rotational temperature analysis, although if it were included it would not change the results significantly.

Under conditions of rotational thermal equilibrium the intensity of a rotational line is given (e.g. Herzberg 1950) as:

$$I_J' \propto \nu^4 S_J' \text{ EXP } (-B'J'(J'+1)\ hc/kT) \qquad (1)$$

where J' is the rotational quantum number for the upper state, ν is the line frequency, and $S_J=J'$ (R branch) or $S_J=J'+1$ (P branch). We take $B'=0.39$ cm^{-1} (Freed et al. 1980). We normalize the observations to the intensity of the R(8) line having J' = 9. We use absolute intensities for each line (discussed below) and we correct each intensity to its value at the sub-solar point using a theoretical model (Deming and Mumma 1983). The fluxes used in the analysis are given in Table I. The resulting rotational temperature for the Martian mesosphere is T_{rot} = 135±20K, and the analysis is illustrated on Fig. 3.

c) Absolute flux measurements

It is important to derive an observed value for the absolute total flux emitted in the 9.4μm and 10.4μm bands. Theoretical modelling of the emission process can predict a value for this flux, and comparison between observed and theoretical fluxes can shed light on the completeness of our understanding. In principle, the observed total flux can be obtained by observing the emission in each rotational line of each band and summing the observed values. This procedure is impractical because of the length of time required to observe a single rotational line with appropriate calibration. We therefore assume rotational thermal equilibrium at T=126K, as in (1), and we derive the total emitted flux by scaling that which is observed for a single line. We assume that the 9.4 and 10.4μm bands emit equally. This assumption is crudely consistent with our observations, and is prescribed more precisely by laboratory measurements of transition rates (Murray, Kruger and Mitchner 1974). We note that the observations of each line give a specific intensity (ergs cm^{-2} sec^{-1} sr^{-1}), which we wish to integrate over solid angle to obtain an emergent flux (ergs cm^{-2} sec^{-1}). To accomplish this, we let θ_E = the angle between an observed ray and a line normal to the atmosphere. We let θ_S = the zenith angle of the sun at the observed position. We denote the emergent specific intensity as $I_\nu(\theta_E,\theta_S)$, and we assume that $I_\nu(\theta_E,\theta_S)$ is independent of azimuthal angle ϕ. An increment of solid angle, $d\omega$, is given as $d\omega = \sin\theta_E d\theta_E d\phi$ and so the emergent flux is

$$f_\nu(\theta_S) = \int_0^{2\pi} d\phi \int_0^{\pi/2} I_\nu(\theta_E,\theta_S) \sin\theta_E \cos\theta_E \, d\theta_E \qquad (2)$$

We expect that $I_\nu(\theta_E,\theta_S) \sim I_\nu(0,\theta_S)/\cos\theta_E$,

hence we obtain

$$f_\nu(\theta_S) = 2\pi I_\nu(0,\theta_S) \qquad (3)$$

Observed values of $I_\nu(\theta_E,\theta_S)$ are given in Tables I and II. Since we expect that the emission intensity will depend on solar zenith distance (θ_S), we use the predictions of the theoretical models to correct the observed values of $I_\nu(\theta_E,\theta_S)$ to the sub-solar point ($\theta_S=0$). We similarly correct these values to $\theta_E=0$, and we give the resultant $I_\nu(0,0)$ values in Tables I and II.

In the case of Mars we observed near opposition, and so $\theta_E \sim \theta_S \sim 0$ at disk center. This means that the corrections to convert $I_\nu(\theta_E,\theta_S)$ to $I_\nu(0,0)$ are small and the resultant $I_\nu(0,0)$ values are not significantly model dependent. For the 10.33μm R(8) line we obtain $I_\nu(0,0) = 2.84 \times 10^{-2} \pm 0.34 \times 10^{-2}$ ergs cm^{-1} sec^{-1} sr^{-1}. This gives $f_\nu(0) = 1.78 \times 10^{-1}$ ergs cm^{-2} sec^{-1} for this line. We denote the total flux emergent in both bands as $F_\nu(\theta_S)$. Adopting T = 126K, we calculate $F_\nu(0) = 13.7\pm1.6$ ergs cm^{-2} sec^{-1}. Our observations, however, were made near aphelion (1.66 a.u.) and the emission strength should be proportional to the incident solar flux. Correcting the emergent flux to the mean distance of 1.52 a.u. we obtain $F_\nu(0) = 16.2\pm1.9$ ergs cm^{-2} sec^{-1}. Random errors in the observed emission intensities are the dominant source of uncertainty in $F_\nu(0)$.

In the case of Venus, the observing geometry creates more difficulty in correcting $I_\nu(\theta_E, \theta_S)$ to $I_\nu(0,0)$. In this case, it seems preferable to use only the 10.33μm R(8) observations taken at 30^0 and 45^0 West. With this restriction we have $I_\nu(0,0) = 8.33 \times 10^{-2}$ ergs cm^{-2} sec^{-1} sr^{-1}. Adopting T = 204K, from the kinetic width of the emission cores, we obtain $F_\nu(0) = 56.2$ ergs cm^{-2} sec^{-1} sr^{-1}. If, in contrast, we use all of the $I_\nu(0,0)$ values for 10.33μm R(8) we obtain $I_\nu(0,0) = 6.93 \pm 0.48 \times 10^{-2}$ and $F_\nu(0) = 46.7 \pm 3.2$ ergs cm^{-2} sec^{-1}. The former value is preferable since it will be less model-dependent and less prone to systematic error.

d) Center-to-limb dependence of the emission

One of the primary motivations for these observations was the hope that the center-to-limb dependence of the emission could be determined with sufficient accuracy to place meaningful constraints on theoretical models of the emission process. Our observations of the center-to-limb dependence are

given in Tables I and II as ratios of the emission intensity observed at each point relative to some normalization point. In the case of Mars this normalization point was taken at disk center. In the case of Venus the normalization point for the 10.33μm observations was the 30° west observation. The 9.34μm Venus observations were normalized to the average of the two west limb observations. For each observed point, Tables I and II give values of cos θ_E and cos θ_S. We have also calculated theoretical values for the intensity at each point, relative to the normalization point. In calculating these theoretical ratios, Mars was represented by the 120K model. If we define I_ν (0,0) = 1.0, inspection of the theoretical models showed that $I_\nu(\theta_E,\theta_S) \approx I_\nu$ $(0,\theta_S)\ I_\nu\ (\theta_E,0)$. Values of $I_\nu\ (0,\theta_S)$ and $I_\nu(\theta_E,0)$ were tabulated in the theoretical models. Using this procedure we calculated $I_\nu(\theta_E,\theta_S)$ for each point of the planetary disk which fell within the heterodyne field of view. The resulting theoretical intensities were convolved with the Airy pattern which represents the diffraction-limited beam pattern of the heterodyne spectrometer. Modelled relative intensities calculated in this manner are given in Tables I and II.

The observed relative intensities are plotted versus the modelled values on Fig. 4. The typical error bars which are given account for error in the observed relative intensities as well as error in the modelled values. Estimate of the latter error is based on a ± 1 arc-sec uncertainty in the position which was observed. Given the estimated random errors, the agreement between the observations and the model is good. However, systematic errors are more difficult to assess. Systematic errors could arise because we determined the position of the instrument beam by visually positioning the planetary image on a cross line reticle. Since subjective judgement is involved in this process, and since a variety of observers participated, systematic departure from our assumed positions is possible.

Fig. 4 represents an improvement on the less quantitative comparisons given by Betz (1976) and Johnson et al. (1976). The principal value of Fig. 4 is that it implies that the strength of the emission is indeed closely proportional to incident solar flux, i.e. that the theoretical values of I_ν (0, θ_S) are correct. If this were not so, it would not have been possible to

obtain good agreement between the observed and theoretical intensity ratios. With respect to the theoretical modelling of $I_\nu(\theta_E,0)$ values, however, Fig. 4 is less useful. In particular, the observations do not have sufficient angular resolution to resolve the sharp peak in $I_\nu(\theta_E,0)$ which is predicted to occur for $\cos\theta_E \sim 0.2$. In this respect, a more significant test of the models could be obtained using data with much higher spatial resolution.

IV. DISCUSSION

Our measurements of the frequency width of the emission give a mean temperature of 126±6K for the Martian mesosphere near 70 km. This determination is in agreement with our rotational temperature analysis, which yields 135±20K. These values are somewhat lower than the mean Viking probe results (Seiff and Kirk 1977), which give ~139K, and the stellar occultation results of Elliot et al. (1977), which give 145±10K. In the case of Venus, our measurements of the thermal width of the emission give T = 204±10K near 109 km, in agreement with the result from the Pioneer Venus Day Probe (Seiff et al. 1980) at this altitude.

We derive a value of 16.2±1.9 ergs cm^{-2} sec^{-1} emitted at the sub-solar point in the 9.4 and 10.4μm bands from the Martian mesosphere. Our measurements for Venus give a total flux of 56±4 ergs cm^{-2} sec^{-1} emitted in both bands. These measurements are compared to the results of the theoretical models in Table III. The results of Johnson et al. (1976) for Mars are also included in this table. We note that Johnson et al. (1976) give a greater total flux than we obtain in this investigation, and they also obtained a higher kinetic temperature from the frequency width of the emission core. Johnson et al. (1976) derive T~170K for the temperature near 75 km, a value which is significantly higher than other measurements have given. The theoretical models, however, show that their measured flux is quite consistent with their measured temperature. Unless this is a coincidence, it suggests that their determination of a 170K mesospheric temperature may represent a genuine mesospheric temperature fluctuation.

The most significant conclusion which can be drawn from Table III is

that the emission observed from Mars is unexpectedly bright. The observed total flux is essentially equal, within the errors, to the flux predicted by the theoretical model. This is surprising, since Deming and Mumma (1983) note that the model makes assumptions which tend to overestimate the emitted flux. In the case of Venus, for example, the observed flux is only 74% of the predicted flux. Betz (1976) and Johnson et al. (1976) have suggested that near-IR absorption by water vapor, followed by resonant vibrational transfer to CO_2, can contribute to the pumping of this emission. This process is not included in the theoretical models, and may account for the differences shown by Table III. A final understanding of the 10μm CO_2 emission is therefore tied to a more comprehensive picture of chemical and radiative processes in the mesospheres of Mars and Venus.

ACKNOWLEDGEMENTS

We thank the staff of Kitt Peak National Observatory for their logistical support, and we thank two anonymous referees for their constructive comments.

Figure Captions

Fig. 1 Heterodyne observations, at 5 MHz resolution, of emission in the 10.33mm R(8) line of CO_2 on Venus. The phase of the planet at the time of observation was 0.5 and the sub-solar point occurs at the (leftmost) limb. The intensity scale is normalized so that the 10μm continuum (~235K) has a value of unity when observed at normal incidence. The spatial resolution is indicated by the full width of the instrumental beam, to its half-power points (HPBW).

Fig. 2 Example showing observations and modelling of the 10.33μm R(8) line of $^{12}C^{16}O_2$ at the center of the Martian disk. The intensity scale is normalized so that unity represents a brightness temperature of 260K. The top portion shows 25 MHz data and modelled profiles; the bottom portion of the figure includes the 5 MHz observations of the emission core.

Fig. 3 Rotational temperature analysis of the laser emission from the Martian mesosphere.

Fig. 4 Comparison of theoretical and observational intensities for the laser emission. The data plotted is from Tables I and II. The abscissa gives the logarithm of the ratio of the intensity at an observed point to the intensity at a normalization point. The ordinate gives the theoretical value of this ratio calculated from the models. Typical error bars are shown; errors for individual points will vary depending on the details of the observing geometry.

REFERENCES

Barker, E. S. (1975). Observations of Venus Water Vapor over the Disk of Venus: The 1972-74 Data Using the H_2O Lines at 8197 A^o and 8176 A^o. Icarus. 25, 268-281.

Betz, A. L. (1976) Ph.D. Thesis, University of California at Berkeley.

Betz, A. L., M. A. Johnson, R. A. McLaren, and E. C. Sutton (1976). Heterodyne detection of CO_2 emission lines and wind velocities in the atmosphere of Venus. Astrophys. J. 208, L141-L144.

Deming, D., F. Espenak, D. Jennings, T. Kostiuk, and M. Mumma (1982). Evidence for high-altitude haze thickening on the dark side of Venus from 10-Micron Heterodyne Spectroscopy of CO_2. Icarus 49, 35-48.

Deming, D. and M. J. Mumma (1983). Modelling of the 10-Micrometer Natural Laser Emission from the Mesospheres of Mars and Venus. Accompanying paper.

Elliot, J. L., R. G. French, E. Dunham, P. J. Gierasch, J. Veverka, C. Church and C. Sagan (1977). Occultation of ε Geminorum by Mars. II. The Structure and Extinction of the Martian Upper Atmospheres. Ap.J. 217, 661-679.

Farmer, C. B., D. W. Davies, A. L. Holland, D. D. LaPorte and P. E. Doms (1977). Mars: Water Vapor Observations from the Viking Orbiters. J. Geophys. Res. 82, 4225-4248.

Freed, C., L. C. Bradley and R. G. O'Donnell (1980). Absolute Frequencies of Lasing Transitions in Seven CO_2 Isotopic Species. IEEE J. Quantum Electronics 16, 1195.

Herzberg, G. (1950). Molecular Spectra and Molecular Structure, Van Nostrand

Reinhold, New York.

Hess, S. L., J. A. Ryan, J. E. Tillman, R. M. Henry and C. B. Leavy (1980). The Annual Cycle of Pressure on Mars Measured by Viking Landers 1 and 2. Geophys. Res. Lett. 7, 197-200.

Johnson, M. A., A. L. Betz, R. A. McLaren, E. C. Sutton and C. H. Townes (1976). Nonthermal 10-micron CO_2 emission lines in the atmospheres of Mars and Venus. Astrophys. J. 208, L145-L148.

Kostiuk, T., M. J. Mumma, and D. Zipoy (1980) Optical considerations in infrared heterodyne spectrometer design. In Heterodyne Systems and Technology, NASA Conference Pub. Vol. 2, pp. 365-

McClatchey, R. A., W. S. Benedict, S. A. Clough, D. E. Burch, R. F. Calfee, K. Fox, L. S. Rothman, and J. S. Garing (1973). AFCRL atmospheric absorption line Parameters Compilation, Reinhold, AFCRL-TR-73-0096.

Montgomery, C. G., J. M. Saari, R. W. Shorthill, N. F. Six, Jr. (1966). Directional Characteristics of Lunar Thermal Emission, Tech. Note R-213, Brown Engineering Co., Inc. Huntsville, Alabama; Boeing Document D1-8L-0568.

Mumma, M. J., D. Buhl, G. Chin, D. Deming, F. Espenak, T. Kostiuk and D. Zipoy (1981), Discovery of natural gain amplification in the 10μm CO_2 laser bands on Mars: a natural laser. Science 212, 45-49.

Mumma, M. J., T. Kostiuk, D. Buhl, G. Chin and D. Zipoy (1982). Infrared heterodyne spectroscopy. Optical Engineering 21, 313-319.

Murray, E. R., C. Kruger and M. Mitchner (1974). Measurement of 9.6-μm CO_2 laser transition probability and optical broadening cross section. Appl Phys Lett, 24, 180-181.

Seiff, A. (1978). Post-Viking Models for the Structure of the Summer

Atmosphere of Mars, in The Mars Reference Atmosphere, ed. A. Kliore, Jet Propulsion Laboratory, California Institute of Technology, Pasadena, California.

Seiff, A. and D. B. Kirk (1977). Structure of the Atmosphere of Mars in Summer at Mid-Latitudes. J. Geophys. Res. 82, 4364-4378.

Seiff, A., D. B. Kirk, R. E. Young, R. C. Blanchard, J. T. Findlay, G. M. Kelly (1980). Measurement of Thermal Structure and Thermal Contrasts in the Atmosphere of Venus and Related Dynamical Observations: Results from the Four Pioneer Venus Probes. J. Geophys. Res. 85, 7903-7933.

Sutton, E. C., W. V. Storey, A. L. Betz and C. H. Townes (1977). Spatial Heterodyne Interferometry of VY Canis Majoris, Alpha Orionis, Alpha Scorpii, and R. Leonis at 11 Microns. Astrophys. J. 217, L97-L100.

Zurek, R. W. (1976). Diurnal tide in the Martian atmosphere. J. Atmos. Sci., 33, 321-337.

TABLE I. Summary of Observations of the laser emission from Mars. Specific intensities are corrected for atmospheric absorption. The specific intensity is a function of angular distance from the sub-earth point, θ_E, and from the sub-solar point, θ_S. Numbers in parentheses are powers of ten.

Date	Time (UT)	Line	Position	Observed Relative Intensity	Predicted Relative Intensity	Kinetic Temperature	Specific Intensity (ergs cm^{-2} sec^{-1} sr^{-1}) $I_\nu(\theta_E,\theta_S)$	$I_\nu(0,0)$	$\cos\theta_E$	$\cos\theta_S$
1/7/80	10:15	10.59μm P(20)	disk center	-	-	-	1.95(-2)	2.18(-2)	1.00	0.85
	12:52	10.33μm R(8)	disk center	-	-	93	3.48(-2)	3.75(-2)	0.99	0.90
2/5/80	04:52	10.33μm R(8)	disk center	-	-	96	2.47(-2)	2.67(-2)	0.94	0.82
	05:16		east limb	1.42	1.24	115	-	-	0.80	0.91
	06:23		west limb	0.94	0.61	136	-	-	0.39	0.14
	06:58		north limb	1.37	1.17	-	-	-	0.47	0.36
	07:35		south limb	0.83	1.20	134	-	-	0.68	0.69
	08:20		disk center	1.00	1.00	128	2.92(-2)	3.03(-2)	0.99	0.95
	09:26	10.30μm R(12)	disk center	-	-	-	2.81(-2)	2.89(-2)	1.00	0.96
	10:00	10.27μm R(16)	disk center	-	-	-	2.58(-2)	2.63(-2)	1.00	0.97
	11:17	10.21μm R(26)	disk center	-	-	-	5.0(-3)	5.1(-3)	0.99	0.98
	14:15	10.37μm R(4)	disk center	-	-	-	3.01(-2)	2.85(-2)	0.92	0.96
3/26/80	05:30	10.33μm R(8)	disk center	1.00	1.00	63	1.98(-2)	2.05(-2)	1.00	0.95
	06:11		east limb	1.43	0.77	158	-	-	0.66	0.36
	06:30		west limb	2.07	1.66	132	-	-	0.60	0.83
	06:55		disk center	-	-	113	3.67(-2)	3.89(-2)	1.00	0.92
3/28/80	03:30	10.33μm R(8)	disk center	-	-	108	1.87(-2)	1.92(-2)	0.99	0.96
	04:00		south limb	0.90	1.05	126	-	-	0.60	0.46
	04:25		north limb	1.11	1.83	119	-	-	0.41	0.55
	04:45		west limb	1.66	2.00	165	-	-	0.48	0.76
	05:55		east limb	0.92	0.59	156	-	-	0.53	0.20

	06:15		disk center	1.00	1.00	134	3.75(-2)	3.95(-2)	1.00	0.93
	07:13		30° east	0.93	0.84	109	-	-	0.76	0.49
	07:35		30° west	1.19	1.23	106	-	-	0.88	0.99
	07:59		30° north	1.06	1.12	126	-	-	0.85	0.83
	08:23		30° south	0.99	0.96	130	-	-	0.88	0.71
3/29/80	04:12	9.32μm R(12)	disk center	1.00	1.00	-	-	-	1.00	0.95
	04:42		west limb	1.45	1.82	-	-	-	0.59	0.84
	05:16		east limb	0.66	0.79	-	-	-	0.66	0.35
	05:39		north limb	1.69	0.85	-	-	-	0.54	0.62
	05:56		south limb	0.92	1.02	-	-	-	0.68	0.52
	07:49	9.34μm R(8)	disk center	1.00	1.00	-	-	-	0.99	0.90
	08:28		west limb	1.91	1.38	-	-	-	0.77	0.95
	09:26		north limb	1.96	1.43	-	-	-	0.24	0.26
	09:54		south limb	1.91	0.87	-	-	-	0.74	0.48
3/30/80	09:30	10.33μm R(8)	disk center	1.00	1.00	132	1.31(-2)	1.52(-2)	0.95	0.81
	09:46		west limb	1.90	1.31	197	-	-	0.85	0.99
4/19/80	05:00	10.33μm R(8)	disk center	1.00	1.00	-	-	-	1.00	0.90
	06:53		west limb	2.50	1.44	-	-	-	0.73	0.95

Table II. Summary of Observations of the laser emission from Venus. Specific intensities are corrected for atmospheric absorption. The specific intensity is a function of angular distance from the sub-earth point, θ_E, and from the sub-solar point, θ_S. Numbers in parentheses are powers of ten.

Date	Time (UT)	Line	Position	Observed Relative Intensity	Predicted Relative Intensity	Kinetic Temperature	Specific Intensity (ergs cm^{-2} sec^{-1} sr^{-1}) $I_\nu(\theta_E, \theta_S)$	$I_\nu(0,0)$	$\cos\theta_E$	$\cos\theta_S$
4/8/80	21:23	10.33μm R(8)	west limb	2.83	3.14	171	1.64(-1)	7.00(-2)	0.42	0.91
	22:05		30° west	1.00	1.00	-	5.80(-2)	7.77(-2)	0.87	0.50
	23:40		west limb	2.95	3.14	185	1.71(-1)	7.30(-2)	0.42	0.91
4/9/80	00:49		southwest limb	1.93	2.60	209	1.12(-1)	5.77(-2)	0.42	0.64
	01:47		south limb	0.51	0.80	-	2.98(-2)	4.99(-2)	0.42	0.08
4/10/80	00:17	9.34μm R(8)	west limb	1.09	1.00	223	-	-	0.42	0.91
	02:01		disk center	0.24	0.10	-	-	-	0.98	0.08
	04:07		south limb	0.26	0.25	-	-	-	0.42	0.08
4/10/80	20:27	9.34μm R(8)	west limb	0.91	1.00	184	-	-	0.42	0.91
	22:42		southwest limb	0.87	0.83	245	-	-	0.42	0.64
4/11/80	00:18	10.33μm R(8)	west limb	2.76	3.14	209	1.60(-1)	6.83(-2)	0.42	0.91
	03:06		disk center	0.33	0.31	-	-	-	0.98	0.08
	03:52		45° west	1.76	1.54	-	1.02(-1)	8.88(-2)	0.71	0.71

Table III. Theoretical and observed values of the total flux emergent in the 9.4μm and 10.4μm bands.

	Observed	Theoretical
	ergs cm^{-2} sec^{-1}	ergs cm^{-2} sec^{-1}
Mars	16±2 (1)	15.1 (126K) (3)
	20 (2)	20.6 (170K)
Venus	56±4 (1)	75.3

(1) This work

(2) Johnson et al. (1976)

(3) Obtained by interpolating between the theoretical values at 120K and 170K.

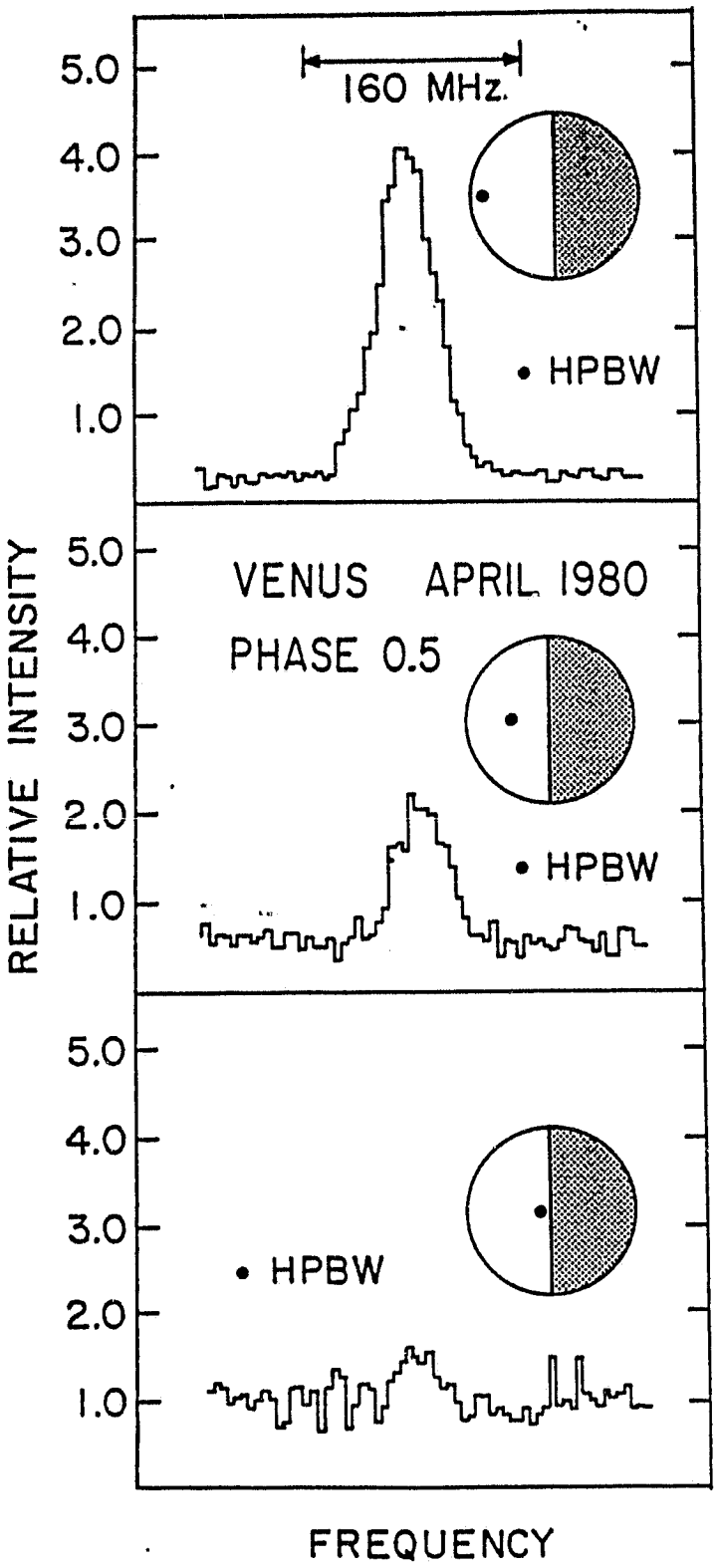

Fig. 1

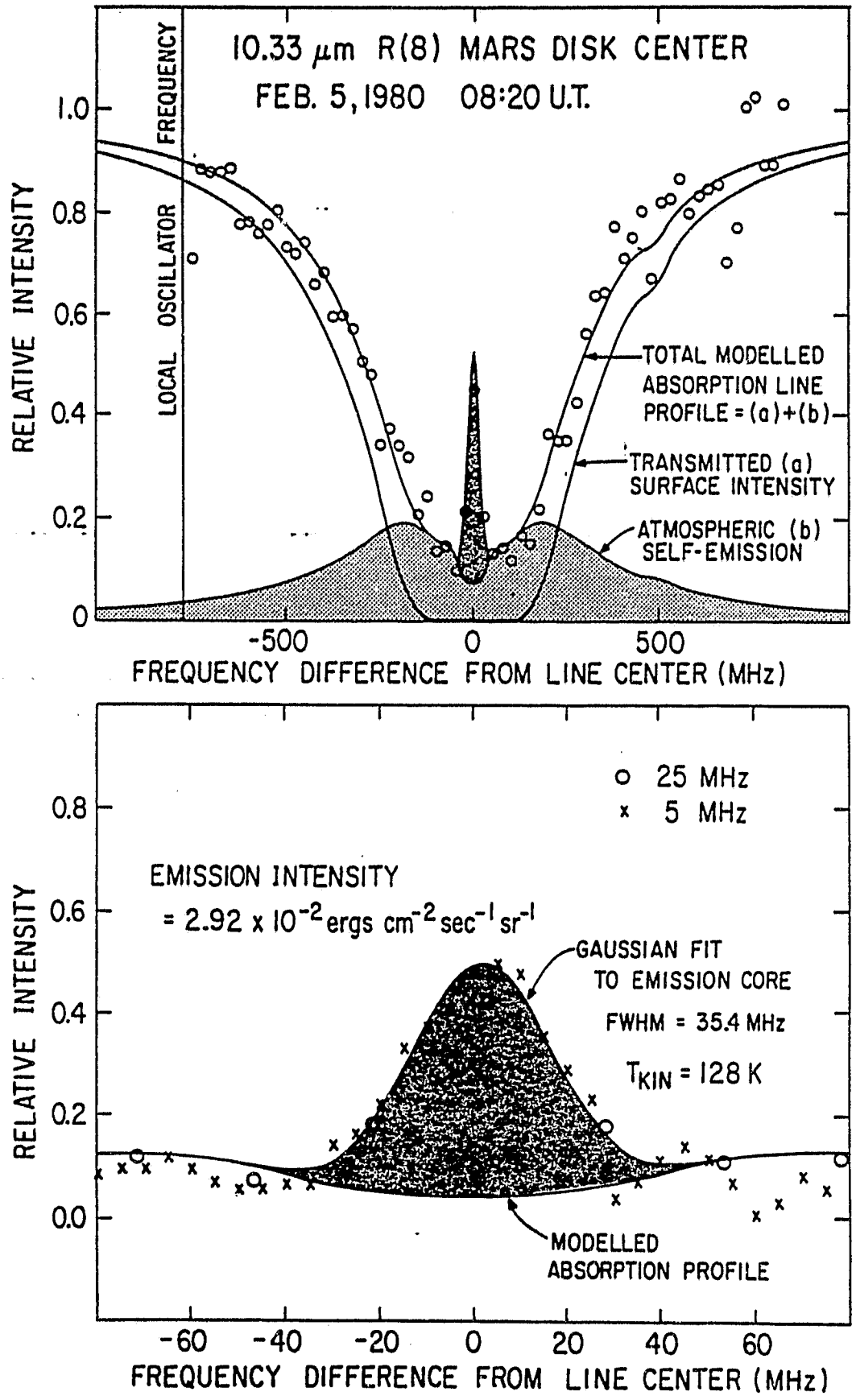

Fig. 2

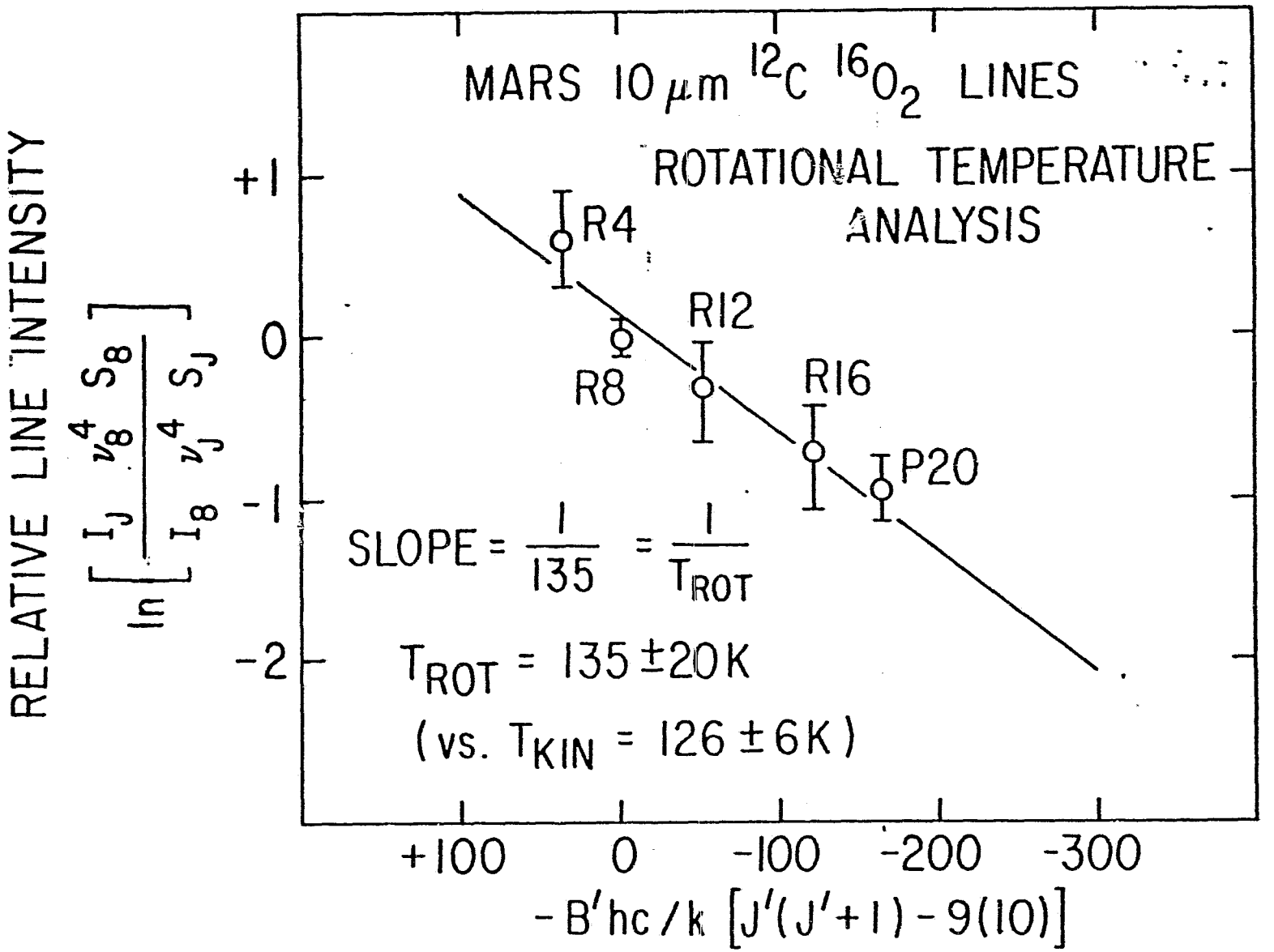
MARS 10 μm $^{12}C\,^{16}O_2$ LINES
ROTATIONAL TEMPERATURE ANALYSIS
R4
R8
R12
R16
P20
SLOPE = 1/135 = 1/T_{ROT}
T_{ROT} = 135 ± 20K
(vs. T_{KIN} = 126 ± 6K)
RELATIVE LINE INTENSITY
$\ln\left[\frac{I_J\ \nu_8^4\ S_8}{I_8\ \nu_J^4\ S_J}\right]$
+1
0
-1
-2
+100
0
-100
-200
-300
$-B'hc/k\,[J'(J'+1)-9(10)]$

Fig. 3

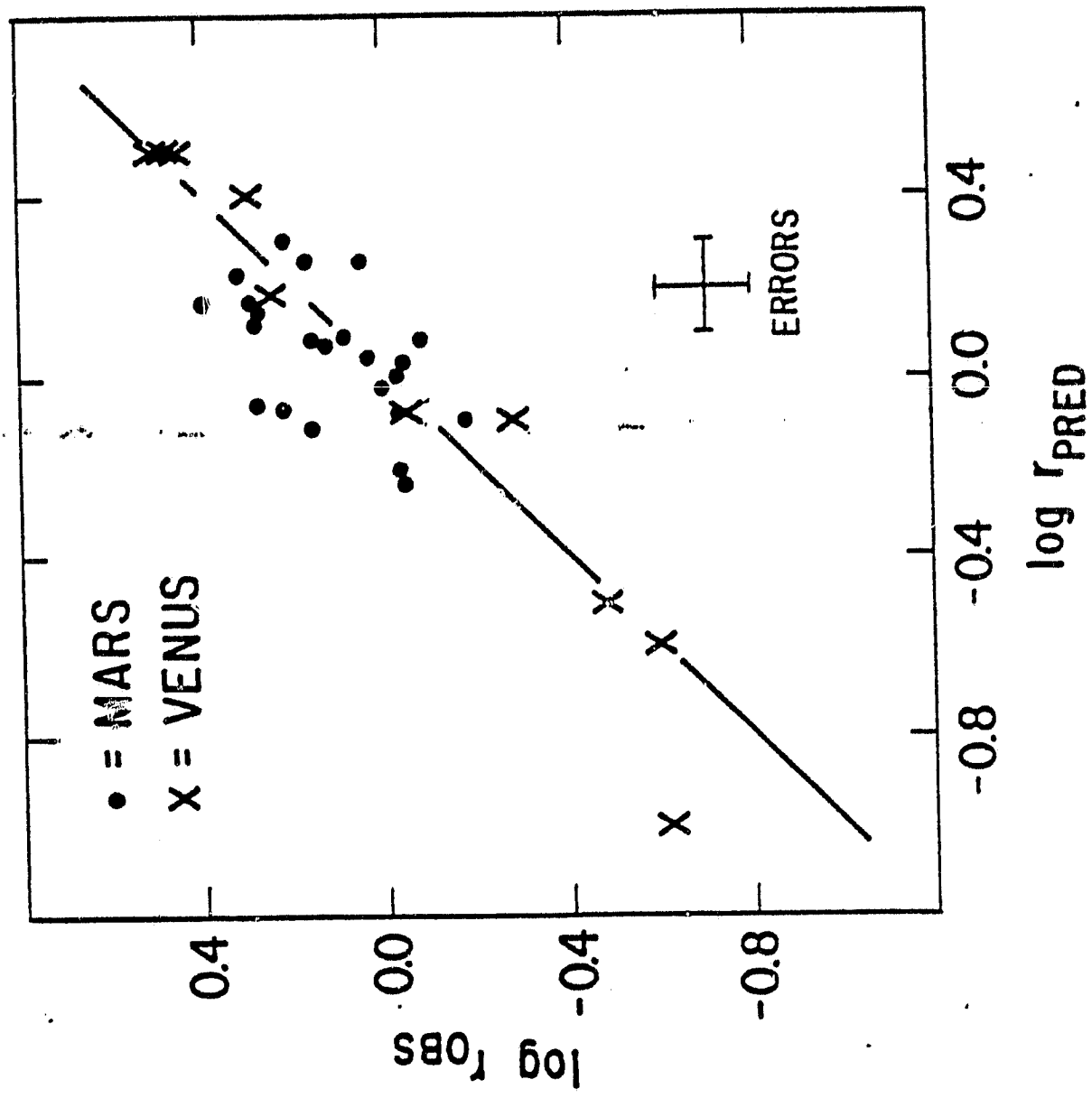

Fig. 5